Soft Gluon Resummation Effects in Single Slepton Production at Hadron Colliders

Li Lin Yang,* Chong Sheng Li,† Jian Jun Liu,‡ and Qiang Li

Department of Physics, Peking University, Beijing 100871, China

(Dated: February 2, 2008)

Abstract

We investigate QCD effects in the production of a single slepton at hadron colliders in the Minimal Supersymmetric Standard Model without R-parity. We calculate the total cross sections and the transverse momentum distributions at next-to-leading order in QCD. The NLO corrections enhance the total cross sections and decrease the dependence of the total cross sections on the factorization and renormalization scales. For the differential cross sections, we resum all order soft gluon effects to give reliable predictions for the transverse momentum distributions. We also compare two approaches to the non-perturbative parametrization and found that the results are slightly different at the Tevatron and are in good agreement at the LHC. Our results can be useful to the simulation of the events and to the future collider experiments.

PACS numbers: 12.38.Cy, 13.85.Qk, 14.80.Ly

*Electronic address: llyang@pku.edu.cn

†Electronic address: csli@pku.edu.cn

‡Present address: Department of Physics, Tsinghua University, Beijing 100084, China

I. INTRODUCTION

The Minimal Supersymmetric Standard Model (MSSM) is one of the most popular new physics models beyond the Standard Model (SM). In the MSSM, R-parity conservation is imposed in order to keep the proton stable. R-parity is a discrete symmetry, which is defined to be $R_p \equiv (-1)^{3(B-L)+2S}$, where B, L and S are baryon number, lepton number, and spin, respectively. All SM particles have $R_p = 1$, and all superpartners have $R_p = -1$. In consequence, the superpartners can only be produced in pair, and the lightest superpartner (LSP) is stable. However, proton decay may be avoided by assuming B or L conservation, but not both. In these cases, R-parity can be violated. For a recent review of the R-parity violating ($\not{R}_p$) extension of the MSSM, see Ref. [1].

The most general form for the $\not{R}_p$ part of the superpotential is

$$W_{\not{R}_p} = \mu_i L_i H_2 + \frac{1}{2}\lambda_{ijk} L_i L_j E^c_k + \lambda'_{ijk} L_i Q_j D^c_k + \frac{1}{2}\lambda''_{ijk} U^c_i D^c_j D^c_k, \tag{1}$$

where $L_i(Q_i)$ and $E_i(U_i, D_i)$ are, respectively, the left-handed lepton (quark) $SU(2)$ doublet and right-handed lepton (quark) $SU(2)$ singlet chiral superfields, and $H_{1,2}$ are the Higgs chiral superfields. The indices i, j, k denote generations and the superscript c denotes charge conjugation. As stated before, we require that the lepton number violating part and the baryon number violating part should not exist simultaneously. For the purpose of this paper, we will assume that only the lepton number violating couplings λ'_{ijk} are non-zero. A recent summary of the bounds on the couplings in Eq. (1) can be found in Ref. [2].

The $\not{R}_p$-MSSM has the remarkable feature that sparticles need not be produced in pair. Therefore, a definitive signal of R-parity violation will be the observation of single sparticle production. The terms in Eq. (1) will result in various resonant sparticle production processes. The term involving λ_{ijk} leads to resonant sneutrino production at e^+e^- colliders [3], while the λ''_{ijk} term leads to resonant squark production in hadron-hadron collisions [4, 5]. The term with λ'_{ijk} can induce both resonant squark production at ep colliders [6] and resonant slepton production at hadron-hadron colliders [4, 7, 8]. We will consider the last case in the following.

The resonant production of a single slepton can lead to interesting phenomenology at hadron colliders. A charged slepton can decay into a neutralino and a charged lepton, and the neutralino can subsequently decay into a charged lepton and two jets via λ' couplings.

Due to the Majorana nature of the neutralino, the two leptons can have either opposite or same charges. The case of two leptons of the same charges is more interesting due to the absence of large SM background. For a detailed analysis of the signal and the background, see Ref. [8]. For a sneutrino, the decay products can be a chargino and a charged lepton. With the subsequent decay of the chargino, the final state could contain three charged leptons which is also a clean signature.

The analysis in the above is all based on the tree-level cross sections. It is well known that in order to reduce the scale dependence of the cross section and get more precision predictions, one must include the QCD radiative corrections. The next-to-leading order QCD corrections to the total cross sections have been calculated in Ref. [9]. However, they used rather old parton distribution functions in the numerical calculations, and their results have large dependence on the PDF sets used. Moreover, they did not consider the kinematic distribution of the events, which is very important in designing the strategy of discovery. In this paper, we will calculate the transverse momentum distribution of the slepton at next-to-leading order in QCD, and also calculate all order soft gluon resummation effects to give reasonable predictions. In our numerical evaluations, we will use the new sets of PDFs, and compare our predictions for the total cross sections with those of Ref. [9].

The paper is organized as follows. Section II describes the production processes at hadron/parton level and shows the leading order (LO) cross sections. Section III presents the analytical expression of the next-to-leading order (NLO) corrections to the cross sections. Section IV gives the analytical and numerical results for the total cross sections and Section V gives the transverse momentum distribution. And finally is the summary.

II. THE PROCESSES AND THE CROSS SECTIONS

We consider the process $A(p_1) + B(p_2) \to L(q) + X$, where A and B are the incoming hadrons (proton-antiproton for Tevatron or proton-proton for LHC) with momenta p_1 and p_2, L stands for charged slepton $\tilde{l}$ (or sneutrino $\tilde{\nu}$) with momentum q. At parton level, four kinds of subprocesses can be induced by the λ'_{ijk} couplings at tree level: $d_k + \bar{u}_j \to \tilde{l}_i$, $d_j + \bar{d}_k \to \tilde{\nu}_i$, and their charge conjugated processes.

In the QCD improved parton model, the hadronic differential cross section can be factorized into the convolution of the partonic differential cross sections with appropriate parton

distribution functions (PDFs):

$$\frac{\mathrm{d}\sigma^{AB}}{\mathrm{d}q_T^2\mathrm{d}y} = \sum_{\alpha,\beta}\int \mathrm{d}x_1\mathrm{d}x_2 \frac{\mathrm{d}\hat{\sigma}^{\alpha\beta}}{\mathrm{d}q_T^2\mathrm{d}y} f_{\alpha/A}(x_1,\mu_f) f_{\beta/B}(x_2,\mu_f), \tag{2}$$

where $\hat{\sigma}^{\alpha\beta}$ is the cross section for the partonic subprocess $\alpha(\hat{p}_1) + \beta(\hat{p}_2) \to L(q) + X$. $\hat{p}_1$ and $\hat{p}_2$ are the momenta of the incoming partons α, β. The momenta fractions x_1 and x_2 are defined by $x_i = \hat{p}_i/p_i, (i = 1, 2)$. $f_{p/H}(x, \mu_f)$ is the parton distribution function which describes the probability of finding a parton p with momentum fraction x inside the hadron H at factorization scale μ_f. The sum is over all possible initial partons which contribute. For any momentum q, it can be decomposed as

$$q = (q^+, q^-, \boldsymbol{q}_T), \qquad q_T^2 = \boldsymbol{q}_T^2, \tag{3}$$

where $q^\pm = q^0 \pm q^3$, and the rapidity y is defined as

$$y = \frac{1}{2}\ln\frac{q^+}{q^-}. \tag{4}$$

We work in the center-of-mass frame of the colliding hadrons, in which

$$p_1 = (\sqrt{s}, 0, \mathbf{0}_T), \qquad p_2 = (0, \sqrt{s}, \mathbf{0}_T), \tag{5}$$

where $s = (p_1 + p_2)^2$ is the center-of-mass energy squared.

The partonic cross section $\hat{\sigma}^{\alpha\beta}$ can be calculated order by order in perturbation theory. The leading order contribution is the Born level process $\alpha(\hat{p}_1) + \beta(\hat{p}_2) \to L(q)$. Here α and β represent only quarks and anti-quarks. The matrix element is simply

$$\mathcal{M}_B = \lambda'_{ijk}\bar{v}(\hat{p}_2)P_L u(\hat{p}_1) \tag{6}$$

where $P_L = (1 - \gamma^5)/2$, and we have ignored the mixing between the left-handed and right-handed sleptons since they are almost degenerate. The coupling λ'_{ijk} depends on the generations of α, β and L. For simplicity, we will make the subscript implicit below and simply write λ'. The one particle phase space can be written as

$$\begin{aligned}\mathrm{d}\Phi_1 &= \frac{\mathrm{d}^3 q}{(2\pi)^3 2q_0}(2\pi)^4\delta^4(\hat{p}_1 + \hat{p}_2 - q) \\ &= (2\pi)\mathrm{d}q_T^2\mathrm{d}y\,\delta(q_T^2)\delta(\hat{p}_1^+ - q^+)\delta(\hat{p}_2^- - q^-).\end{aligned} \tag{7}$$

After convoluted with the PDFs, the differential cross section with respect to the transverse momentum and rapidity of the slepton is

$$\begin{aligned}\frac{\mathrm{d}\sigma_B}{\mathrm{d}q_T^2\mathrm{d}y} &= \frac{\pi}{m^2 s}\overline{|\mathcal{M}_B|^2}\,\delta(q_T^2) f_{\alpha/A}(x_1^0,\mu_f) f_{\beta/B}(x_2^0,\mu_f) \\ &= \frac{\pi}{12s}\lambda'^2\,\delta(q_T^2) f_{\alpha/A}(x_1^0,\mu_f) f_{\beta/B}(x_2^0,\mu_f),\end{aligned} \tag{8}$$

where $x_1^0 = \sqrt{\tau}e^y$ and $x_2^0 = \sqrt{\tau}e^{-y}$ with $\tau = m^2/s$, and m is the mass of the slepton. We have made the summation over the initial states α, β implicit.

III. NEXT-TO-LEADING ORDER CALCULATIONS

The NLO QCD corrections consist of the following contributions: the exchange of virtual gluons and the corresponding renormalization counterterms, the real gluon emission subprocesses, the gluon initiated subprocesses, and the contributions of Altarelli-Parisi (A-P) splitting functions. In the following, we will calculate these contributions seperately. We use dimensional regularization (DREG) in $d = 4 - 2\epsilon$ dimensions to regulate all divergences and adopt $\overline{\mathrm{MS}}$ renomalization and factorization scheme to remove the ultraviolet (UV) and infrared (IR) (including soft and collinear) divergences.

A. Virtual gluon exchange

Evaluating the relevant Feynman diagrams of virtual corrections, we obtain the amplitude

$$\mathcal{M}_V = \mathcal{M}_B \frac{\alpha_s}{2\pi} C_F (4\pi)^\epsilon \Gamma(1+\epsilon)\left[-\frac{1}{\epsilon^2} - \frac{1}{\epsilon}\ln\frac{\mu_r^2}{m^2} - \frac{1}{2}\ln^2\frac{\mu_r^2}{m^2} + \frac{2\pi^2}{3} - 1\right], \tag{9}$$

where $C_F = 4/3$ and μ_r is the renormalization scale. In order to remove the UV divergences in $\mathcal{M}_V$, a renormalization procedure must be carried out. We define the renormalization constants as

$$\lambda_0' = Z_\lambda \lambda' \mu_r^\epsilon = (1 + \delta Z_\lambda)\lambda' \mu_r^\epsilon, \tag{10}$$

$$\begin{aligned}\psi_0 &= Z_{\psi L}^{1/2}\psi_L + Z_{\psi R}^{1/2}\psi_R \\ &= \left(1 + \frac{1}{2}\delta Z_{\psi L}\right)\psi_L + \left(1 + \frac{1}{2}\delta Z_{\psi R}\right)\psi_R,\end{aligned} \tag{11}$$

where λ_0' and ψ_0 are the bare coupling and the bare quark wave function, respectively. In the $\overline{\rm MS}$ scheme, these renormalization constants are fixed to be

$$\delta Z_{\psi L} = \delta Z_{\psi R} = -\frac{\alpha_s}{4\pi} C_F (4\pi)^\epsilon \Gamma(1+\epsilon) \frac{1}{\epsilon}, \tag{12}$$

$$\delta Z_\lambda = -\frac{\alpha_s}{4\pi} C_F (4\pi)^\epsilon \Gamma(1+\epsilon) \frac{3}{\epsilon}. \tag{13}$$

Thus the running of the coupling constant is governed by

$$\lambda'(\mu) = \frac{\lambda'(\mu_0)}{1 + \dfrac{3\alpha_s}{4\pi} C_F \log \dfrac{\mu^2}{\mu_0^2}}. \tag{14}$$

After adding the counter term, the UV divergences in $\mathcal{M}_V$ are cancelled, but the IR divergent terms still persist. The corresponding differential cross section is

$$\frac{{\rm d}\sigma_V}{{\rm d}q_T^2 {\rm d}y} = \frac{{\rm d}\sigma_B}{{\rm d}q_T^2 {\rm d}y} \frac{\alpha_s}{\pi} C_F (4\pi)^\epsilon \Gamma(1+\epsilon) \left[-\frac{1}{\epsilon^2} - \frac{1}{\epsilon}\left(\frac{3}{2} + \ln\frac{\mu_r^2}{m^2}\right) - \frac{1}{2}\ln^2\frac{\mu_r^2}{m^2} + \frac{2\pi^2}{3} - 1 \right]. \tag{15}$$

B. Real gluon emission

We now consider the contribution from the emission of one gluon $\alpha(\hat{p}_1) + \beta(\hat{p}_2) \to L(q) + g(k)$. We define the Mandelstam variables as

$$\begin{aligned}
s &= (p_1 + p_2)^2, \\
t &= (p_1 - q)^2 = m^2 - p_1^+ q^- = m^2 - \sqrt{s(q_T^2 + m^2)} e^{-y}, \\
u &= (p_2 - q)^2 = m^2 - p_2^- q^+ = m^2 - \sqrt{s(q_T^2 + m^2)} e^{y}, \\
\hat{s} &= (\hat{p}_1 + \hat{p}_2)^2 = x_1 x_2 s, \\
\hat{t} &= (\hat{p}_1 - q)^2 = x_1(t - m^2) + m^2, \\
\hat{u} &= (\hat{p}_2 - q)^2 = x_2(u - m^2) + m^2.
\end{aligned} \tag{16}$$

The squared matrix element (with spin and color summed and averaged) can be expressed as

$$\begin{aligned}
\overline{|\mathcal{M}_R|^2} &= \frac{8}{9}\pi\alpha_s \lambda'^2 \mu_r^{2\epsilon} \frac{(1-\epsilon)(\hat{s}^2 + m^4) + 2\epsilon \hat{s} m^2}{\hat{t}\hat{u}} \\
&= \frac{8}{9}\pi\alpha_s \lambda'^2 \mu_r^{2\epsilon} x_1 x_2 s \frac{1}{q_T^2} \left\{ (1-\epsilon)\left[1 + \left(\frac{\tau}{x_1 x_2}\right)^2\right] + 2\epsilon \frac{\tau}{x_1 x_2} \right\}.
\end{aligned} \tag{17}$$

The two particle phase space in d dimensions is

$$\begin{aligned}
\mathrm{d}\Phi_2 &= \frac{\mathrm{d}^{d-1}q}{(2\pi)^{d-1}2q_0}\frac{\mathrm{d}^{d-1}k}{(2\pi)^{d-1}2k_0}(2\pi)^d\delta^d(\hat{p}_1+\hat{p}_2-q-k) \\
&= \frac{1}{2(2\pi)^{d-2}}\mathrm{d}^{d-2}\boldsymbol{q}_T\mathrm{d}y\,\delta(\hat{s}+\hat{t}+\hat{u}-m^2) \\
&= \frac{1}{8\pi}\frac{1}{\Gamma(1-\epsilon)}\left(\frac{4\pi}{q_T^2}\right)^{\epsilon}\mathrm{d}q_T^2\mathrm{d}y\,\delta(\hat{s}+\hat{t}+\hat{u}-m^2). \qquad (18)
\end{aligned}$$

Thus the differential cross section can be written as

$$\begin{aligned}
\frac{\mathrm{d}\sigma_R}{\mathrm{d}q_T^2\mathrm{d}y} &= \int \mathrm{d}x_1\mathrm{d}x_2 F(x_1,x_2)\delta(x_1x_2s+x_1(t-m^2)+x_2(u-m^2)+m^2) \\
&= \frac{1}{s}\int_{x_1^-}^1 \frac{\mathrm{d}x_1}{x_1-x_1^+}F(x_1,x_2^*), \qquad (19)
\end{aligned}$$

where

$$\begin{aligned}
x_1^- &= \frac{x_1^+-\tau}{1-x_2^+}, \qquad x_2^* = \frac{x_1x_2^+-\tau}{x_1-x_1^+}, \\
x_1^+ &= e^y\sqrt{\tau+q_T^2/s}, \qquad x_2^+ = e^{-y}\sqrt{\tau+q_T^2/s}, \qquad (20)
\end{aligned}$$

and

$$\begin{aligned}
F(x_1,x_2) = \frac{\alpha_s}{18}\lambda'^2\frac{1}{\Gamma(1-\epsilon)}\left(\frac{4\pi\mu_r^2}{q_T^2}\right)^{\epsilon} & f_{\alpha/A}(x_1,\mu_f)f_{\beta/B}(x_2,\mu_f) \\
\times \frac{1}{q_T^2}\left\{(1-\epsilon)\left[1+\left(\frac{\tau}{x_1x_2}\right)^2\right]\right. & \left.+2\epsilon\frac{\tau}{x_1x_2}\right\}. \qquad (21)
\end{aligned}$$

C. Gluon splitting subprocesses

In addition to the real gluon emission subprocess, there are also contributions from the gluon initiated processes $\alpha(\hat{p}_1)+g(\hat{p}_2)\to L(q)+\bar{\beta}(k)$ and $g(\hat{p}_1)+\beta(\hat{p}_2)\to L(q)+\bar{\alpha}(k)$. Defining the Mandelstam variables as before, for the first subprocesses we can write the the squared matrix elements as

$$\begin{aligned}
\overline{|\mathcal{M}_G^{qg}|^2} &= \frac{1}{3}\pi\alpha_s\lambda'^2\mu_r^{2\epsilon}\frac{(1-\epsilon)(\hat{u}^2+m^4)+2\epsilon\hat{u}m^2}{-(1-\epsilon)\hat{s}\hat{t}} \\
&= \frac{1}{3}\pi\alpha_s\lambda'^2\mu_r^{2\epsilon}x_1x_2s\frac{1}{q_T^2}\left\{\frac{(x_2x_1^+-\tau)[(x_2x_1^+-\tau)^2+\tau^2]}{(x_1x_2)^3}-\frac{2\epsilon}{1-\epsilon}\frac{(x_2x_1^+-\tau)^2\tau}{(x_1x_2)^3}\right\}, \qquad (22)
\end{aligned}$$

while the squared matrix elements for the second subprocess can be obtained from the above one by the substitution $\hat{t} \leftrightarrow \hat{u}$, $x_1 \leftrightarrow x_2$, $x_1^+ \leftrightarrow x_2^+$, namely

$$\begin{aligned}\overline{|\mathcal{M}_G^{gq}|^2} &= \frac{1}{3}\pi\alpha_s\lambda'^2\mu_r^{2\epsilon}\frac{(1-\epsilon)(\hat{t}^2+m^4)+2\epsilon\hat{t}m^2}{-(1-\epsilon)\hat{s}\hat{u}} \\ &= \frac{1}{3}\pi\alpha_s\lambda'^2\mu_r^{2\epsilon}x_1x_2s\frac{1}{q_T^2}\left\{\frac{(x_1x_2^+-\tau)[(x_1x_2^+-\tau)^2+\tau^2]}{(x_1x_2)^3}-\frac{2\epsilon}{1-\epsilon}\frac{(x_1x_2^+-\tau)^2\tau}{(x_1x_2)^3}\right\}.\end{aligned} \tag{23}$$

Thus the differential cross section is

$$\begin{aligned}\frac{\mathrm{d}\sigma_G}{\mathrm{d}q_T^2\mathrm{d}y} &= \int \mathrm{d}x_1\mathrm{d}x_2F'(x_1,x_2)\delta(x_1x_2s+x_1(t-m^2)+x_2(u-m^2)+m^2) \\ &= \frac{1}{s}\int_{x_1^-}^1\frac{\mathrm{d}x_1}{x_1-x_1^+}F'(x_1,x_2^*),\end{aligned} \tag{24}$$

where

$$\begin{aligned}F'(x_1,x_2) = &\frac{1}{16\pi}\frac{1}{x_1x_2s}\frac{1}{\Gamma(1-\epsilon)}\left(\frac{4\pi}{q_T^2}\right)^\epsilon \\ &\times\left[f_{\alpha/A}(x_1,\mu_f)f_{g/B}(x_2,\mu_f)\overline{|\mathcal{M}_G^{qg}|^2}+f_{g/A}(x_1,\mu_f)f_{\beta/B}(x_2,\mu_f)\overline{|\mathcal{M}_G^{gq}|^2}\right].\end{aligned} \tag{25}$$

D. Splitting function contributions

The contributions from splitting functions are essential to cancel the collinear divergences in the cross sections. They arise from the renormalization of the PDFs at NLO. In the $\overline{\mathrm{MS}}$ scheme, the renormalized PDFs can be expressed as

$$f_{\alpha/H}(x,\mu_f) = f_{\alpha/H}(x)+\sum_\beta\left(-\frac{1}{\epsilon}\right)\frac{\alpha_s}{2\pi}\Gamma(1+\epsilon)\left(\frac{4\pi\mu_r^2}{\mu_f^2}\right)^\epsilon\int_x^1\frac{\mathrm{d}z}{z}P_{\alpha\beta}(z)f_{\beta/H}(x/z), \tag{26}$$

where $P_{\alpha\beta}(z)$ are the A-P splitting functions, which are given by

$$P_{qq}(z) = P_{\bar{q}\bar{q}}(z) = C_F\left[\frac{3}{2}\delta(1-z)+\frac{1+z^2}{(1-z)_+}\right], \tag{27}$$

$$P_{qg}(z) = P_{\bar{q}g}(z) = \frac{1}{2}(z^2+(1-z)^2). \tag{28}$$

The resulting contributions to the differential cross section are

$$\begin{aligned}\frac{\mathrm{d}\sigma_C}{\mathrm{d}q_T^2\mathrm{d}y} = &\frac{\pi}{12s}\lambda'^2\delta(q_T^2)\frac{1}{\epsilon}\frac{\alpha_s}{2\pi}\Gamma(1+\epsilon)\left(\frac{4\pi\mu_r^2}{\mu_f^2}\right)^\epsilon \\ &\times\left[(P\circ f)_{\alpha/A}(x_1^0,\mu_f)f_{\beta/B}(x_2^0,\mu_f)+f_{\alpha/A}(x_1^0,\mu_f)(P\circ f)_{\beta/B}(x_2^0,\mu_f)\right],\end{aligned} \tag{29}$$

where

$$(P \circ f)_{\alpha/H}(x,\mu_f) = \sum_\gamma \int_x^1 \frac{\mathrm{d}z}{z} P_{\alpha\gamma}(z) f_{\gamma/H}(x/z,\mu_f). \tag{30}$$

IV. TOTAL CROSS SECTIONS

The total cross sections can be obtained by integrating out q_T and y from the differential cross sections given above. The leading order result is

$$\sigma_{\rm LO} = \frac{\pi}{12s}\lambda'^2 \int_\tau^1 \frac{\mathrm{d}x}{x} f_{\alpha/A}(x,\mu_f) f_{\beta/B}(\tau/x,\mu_f). \tag{31}$$

The next-to-leading order result can be written as

$$\begin{aligned}\sigma_{\rm NLO} = \int \mathrm{d}x_1 \mathrm{d}x_2 \Big[& \hat{\sigma}^{\alpha\beta} f_{\alpha/A}(x_1,\mu_f) f_{\beta/B}(x_2,\mu_f) \\ & + \hat{\sigma}^{\alpha g} f_{\alpha/A}(x_1,\mu_f) f_{g/B}(x_2,\mu_f) + \hat{\sigma}^{g\beta} f_{g/A}(x_1,\mu_f) f_{\beta/B}(x_2,\mu_f) \Big],\end{aligned} \tag{32}$$

where

$$\begin{aligned}\hat{\sigma}^{\alpha\beta} = \frac{\alpha_s}{9\hat{s}}\lambda'^2 \Bigg\{ & \left(\frac{3}{2}\ln\frac{\mu_r^2}{\mu_f^2} + \frac{\pi^2}{3} - 1 \right) \delta(1-z) + \ln\frac{m^2}{\mu_f^2} \frac{1+z^2}{(1-z)_+} \\ & + 2(1+z^2) \left(\frac{\ln(1-z)}{1-z} \right)_+ - (1+z^2)\frac{\ln z}{1-z} + (1-z) \Bigg\},\end{aligned} \tag{33}$$

$$\hat{\sigma}^{\alpha g} = \hat{\sigma}^{g\beta} = \frac{\alpha_s}{48\hat{s}}\lambda'^2 \left[\left(\ln\frac{m^2}{\mu_f^2} + \ln\frac{(1-z)^2}{z} \right) (z^2 + (1-z)^2) + \frac{1}{2}(1-z)(7z-3) \right]. \tag{34}$$

Here $z \equiv \dfrac{m^2}{\hat{s}} = \dfrac{\tau}{x_1 x_2}$, and the function with a subscript "+" is a distribution, which is defined as

$$\int_0^1 \mathrm{d}z g(z) f(z)_+ = \int_0^1 \mathrm{d}z (g(z) - g(1)) f(z) \tag{35}$$

for an arbitrary function $g(z)$. Our expressions for the total cross sections are the same as those obtained in Ref. [9].

In the numerical evaluation of the total cross sections, we use the updated version of the CTEQ and MRST PDF, namely CTEQ6.1 and MRST2004 (there is no update for GRV98 PDF). The renormalization and factorization scale are taken to the mass of the final state slepton, $\mu_r = \mu_f = m$, unless otherwise specified. We will set the initial quarks to only the light flavours u, d and s. Due to the severe constraints on the products of two λ's, we will consider the contributions from one single λ'_{ijk} at a time. The most stringent constraints

on the couplings relevant here come from the rare semileptonic decay $K \to \pi\nu\bar{\nu}$, which gives $\lambda'_{ijk} \leq 0.012 m_{\tilde{d}_k}/(100\text{GeV})$ for $k = 1, 2$. We can assume that the first two generations of sfermions have nearly degenerate masses, so we can take the down squark mass as the slepton mass approximately. In the following, unless otherwise specified, we will take the tree level coupling $\lambda'_{ijk} = 0.01$, which can satisfy the constraints for all the slepton masses under consideration. The cross sections for other values of λ' can be obtained easily by a multiplicative factor.

For convenience, we define three cross sections as following:

$$\begin{aligned}
\sigma_{\text{LO1}}: &\quad \text{LO partonic cross section convoluted with LO PDFs;} \\
\sigma_{\text{LO2}}: &\quad \text{LO partonic cross section convoluted with NLO } (\overline{\text{MS}}) \text{ PDFs;} \\
\sigma_{\text{NLO}}: &\quad \text{NLO partonic cross section convoluted with NLO } (\overline{\text{MS}}) \text{ PDFs,}
\end{aligned}$$

and correspondingly two K factors:

$$K_1 = \frac{\sigma_{\text{NLO}}}{\sigma_{\text{LO1}}}, \qquad K_2 = \frac{\sigma_{\text{NLO}}}{\sigma_{\text{LO2}}}.$$

As the above definitions, K_2 measures only the size of the NLO QCD corrections to the cross sections, while K_1 accounts for the effects of changing parton distribution functions additionally.

A. Sneutrino production

We will consider sneutrino production first. The possible partonic initial states are $d\bar{d}$, $d\bar{s}$, $s\bar{d}$ and $s\bar{s}$.

Fig. 1 shows the cross sections for sneutrino production at the Tevatron as functions of the sneutrino mass. The left and right graphs correspond to CTEQ6.1 and MRST2004 PDFs, respectively. The solid, dashed and dotted curves represents to σ_{NLO}, σ_{LO1} and σ_{LO2}, respectively. For $p\bar{p}$ collision, since we take the λ's to be equal, the cross sections from $s\bar{d}$ initial states are obviously equal to those from $d\bar{s}$ initial states. We find that the NLO QCD corrections generally enhance the total cross sections. The cross sections decrease monotonically with the increasing of the sneutrino mass. From Fig. 1, one can see that, for a sneutrino of mass $m = 200$ GeV, if we take $\lambda' = 0.02$, the leading order (LO1) and the next-leading-order cross sections from $d\bar{d}$ channel are 274 fb and 400 fb, respectively. The

cross sections from $d\bar{s}$ channel are 58 fb and 83 fb, while the ones from $s\bar{s}$ channel are 11 fb and 16 fb, respectively. The cross sections for the LHC case are shown in Fig. 2. For pp

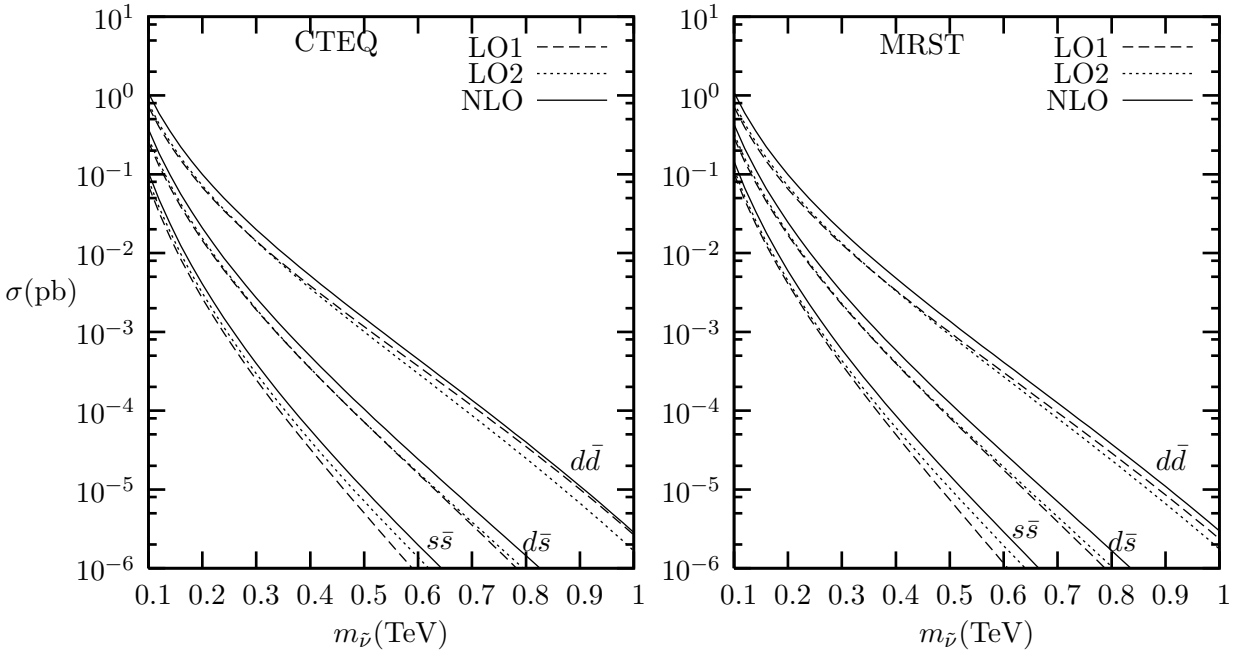

FIG. 1: The cross sections for sneutrino production from various initial states at the Tevatron. The cross sections from $s\bar{d}$ initial states is obviously equal to those from $d\bar{s}$ initial states for $p\bar{p}$ collision if the corresponding λ's are equal.

collider, the cross sections from $d\bar{s}$ and $s\bar{d}$ initial states are no longer equal even with equal couplings. For a 200 GeV sneutrino and $\lambda' = 0.02$, the cross sections from $d\bar{d}$ channel can reach 3.17 pb (LO1) and 4.2 pb (NLO), respectively. The cross sections from other channels are relatively smaller, but still remarkable as the cases at the Tevatron. Our results are consistent with those from Ref. [9].

To quantify the enhancement of the total cross sections by the NLO QCD corrections, we show the K factors in the following. First, we plot K_2 as functions of the sneutrino mass in Fig. 3. The curves are quite similar in spite of different PDF sets and different initial states, which is just a reflection of the flavour blindness of QCD. The solid and dashed curves correspond to CTEQ and MRST PDFs, respectively. For each PDF set, the curves from top to bottom represents $d\bar{d}$, $d\bar{s}$, $s\bar{d}$ and $s\bar{s}$ initiated processes, respectively, while for the Tevatron case $s\bar{d}$ is omitted. The ordering of the magnitudes of the K factors of different initial states is expected, which is due to the different weights of the contributions from

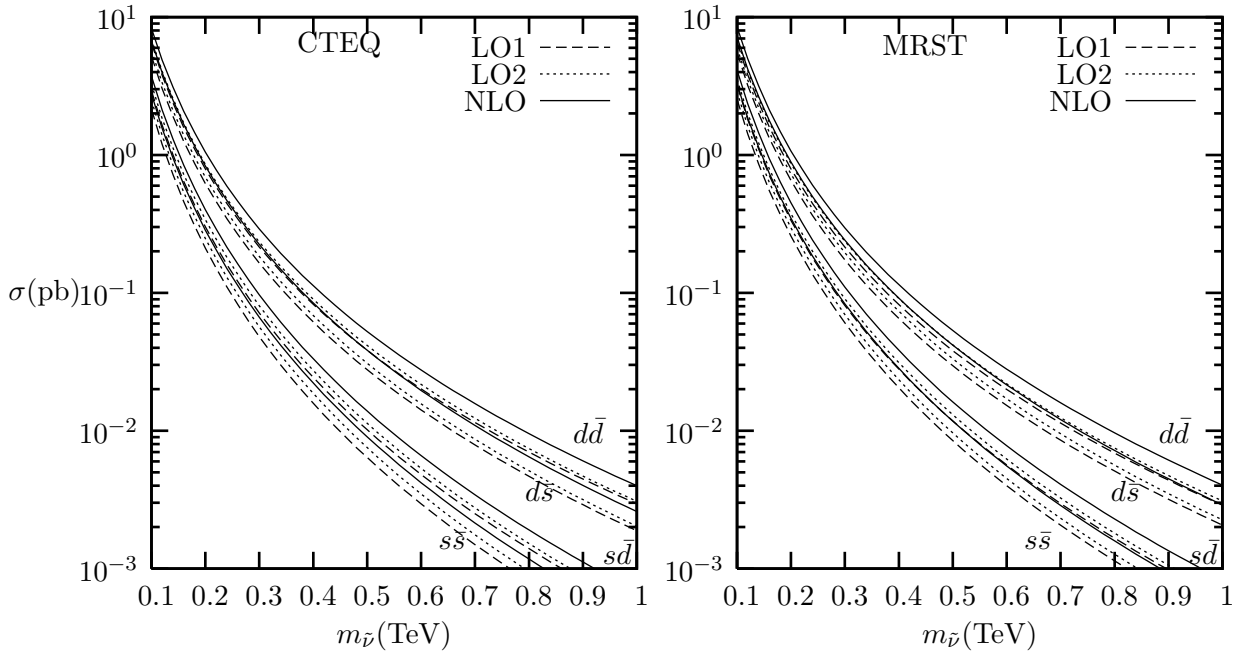

FIG. 2: The cross sections for sneutrino production at the LHC. For pp collision $d\bar{s}$ initiated process has larger cross section than $s\bar{d}$ initiated one if the couplings are the same.

gluon initiated subprocesses. The corrections increase monotonically with the increasing of sneutrino mass, and can reach 70 percent at Tevatron and 30 percent at LHC for a 1 TeV sneutrino, respectively.

The case of K_1 is a bit more complicated due to the different order of PDFs involved. In Fig. 4 we plot K_1 for $d\bar{d}$ initial states as functions of the sneutrino mass. We find that there is still certain discrepancy between the results of CTEQ and MRST parton distributions, especially at large $m_{\tilde{\nu}}$ region. This is mainly due to the difference of the leading order results at region of large momentum fraction, while the next-to-leading order results of the two PDF sets are quite close to each other, as shown in Fig. 1. This confirm the necessity of calculating the NLO corrections. For the subprocesses involving strange quark, we only plot K_1 for $s\bar{s}$ initial states. From Fig. 5 in Ref. [9], one can see that there was large discrepancy between the results of CTEQ5 and MRST98 PDF sets. With the updated PDFs, we find that the discrepancy has been significantly reduced. As shown in Fig. 5, the two curves agree each other quite well, and are more close to the CTEQ5 results given in Ref. [9].

We now investigate the dependence of the cross sections on the renormalization and factorization scales. We will choose the renormalization μ_r and the factorization scale μ_f to

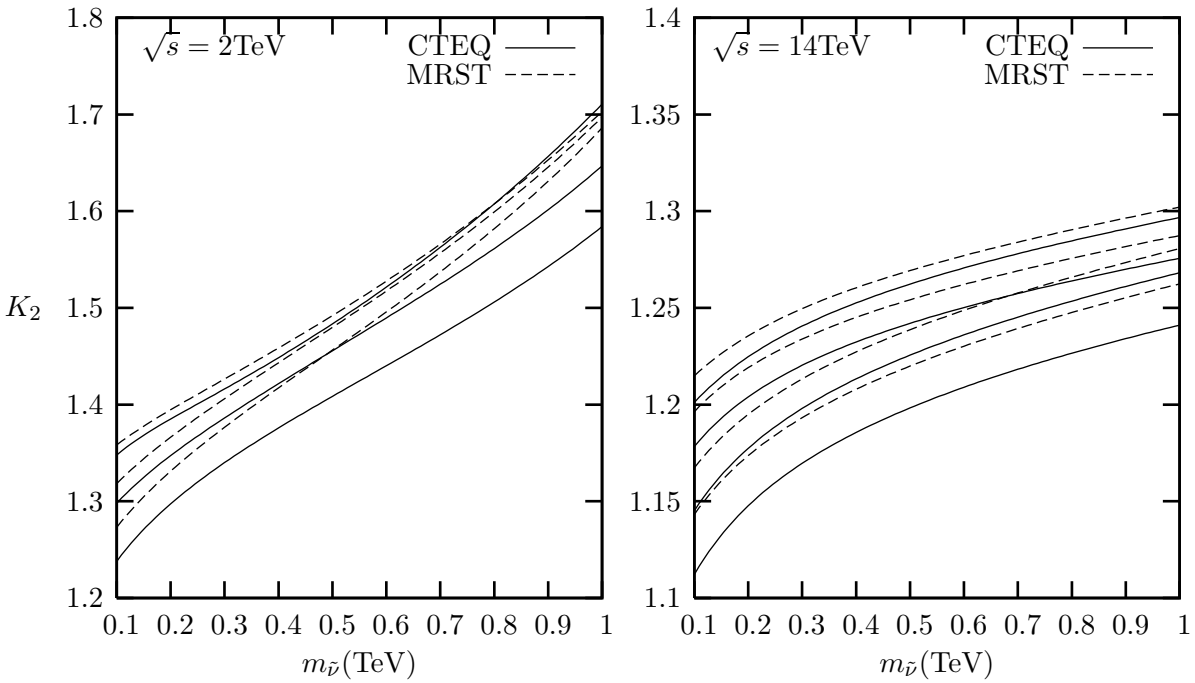

FIG. 3: K_2 for sneutrino production at the Tevatron (left graph) and at the LHC (right graph). The solid and dashed curves correspond to CTEQ and MRST PDFs, respectively. For each PDF set, the curves from top to bottom represents $d\bar{d}$, $d\bar{s}$, $s\bar{d}$ and $s\bar{s}$ initiated processes, respectively, while for the Tevatron case $s\bar{d}$ is omitted.

be equal, $\mu_r = \mu_f = \kappa\mu_0$, where $\mu_0 = m_{\tilde{\nu}}$ is the mass of the sneutrino. In Fig. 6 we plot the ratios of the cross sections $R = \sigma(\kappa)/\sigma(1)$ as functions of κ for $m_{\tilde{\nu}} = 200$ GeV. We only use CTEQ PDFs, since the parametrization of the parton distribution is irrelevant for the main conclusion here. We show here the results of $d\bar{d}$ initial states, and the results of other initial states are similar. From the figure one can see that the dependence on the scales is significantly reduced from LO to NLO, as we expected.

B. Charged slepton production

We now turn to the production of charged sleptons. The possible initial states now become $u\bar{d}$ and $u\bar{s}$ for sleptons with positive charge, $d\bar{u}$ and $s\bar{u}$ for ones with negative charge, respectively. For simplicity, we will only consider contributions from $u\bar{d}$ and $d\bar{u}$ initial states, and only use the CTEQ6.1 PDF. The situation is much similar to the production of sneutrinos, so we do not discuss any details here and just show the cross sections in Fig. 7

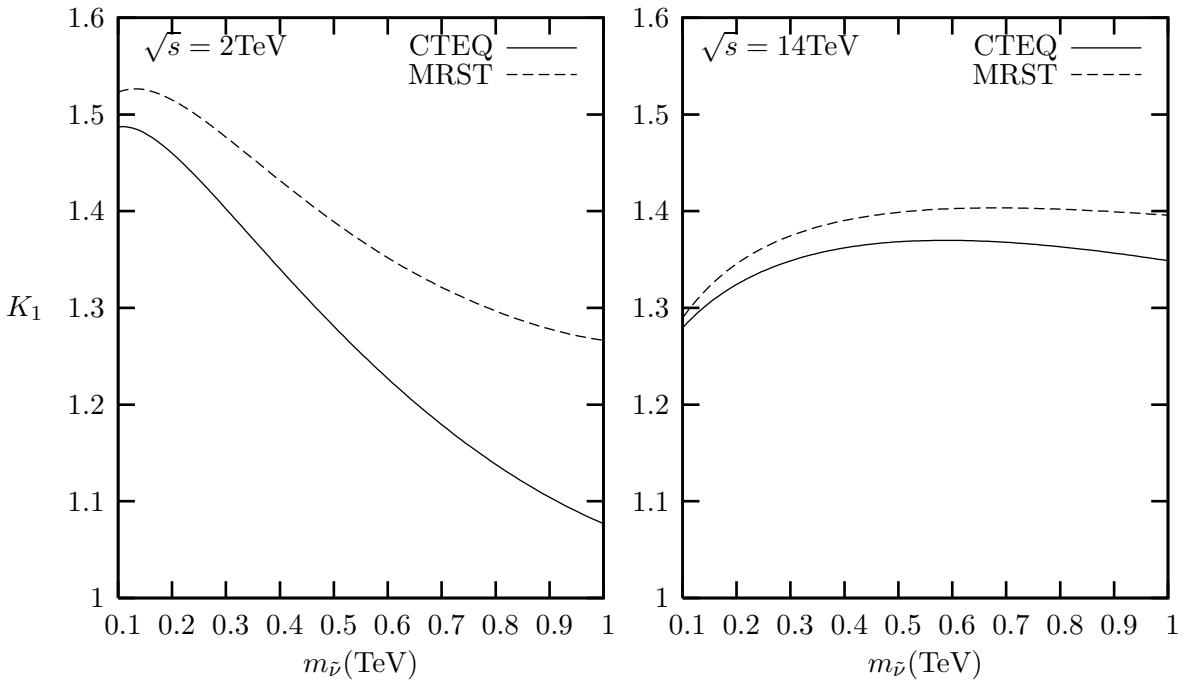

FIG. 4: K_1 for sneutrino production from $d\bar{d}$ initial states at the Tevatron (left graph) and at the LHC (right graph).

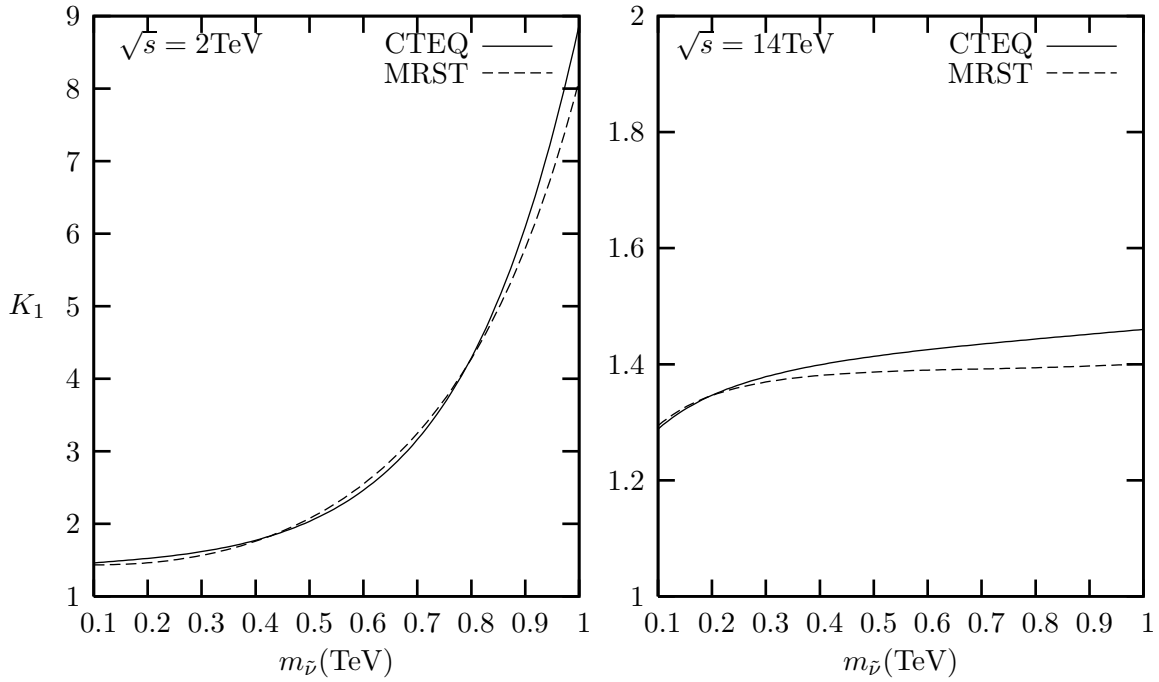

FIG. 5: K_1 for sneutrino production from $s\bar{s}$ initial states at the Tevatron (left graph) and at the LHC (right graph).

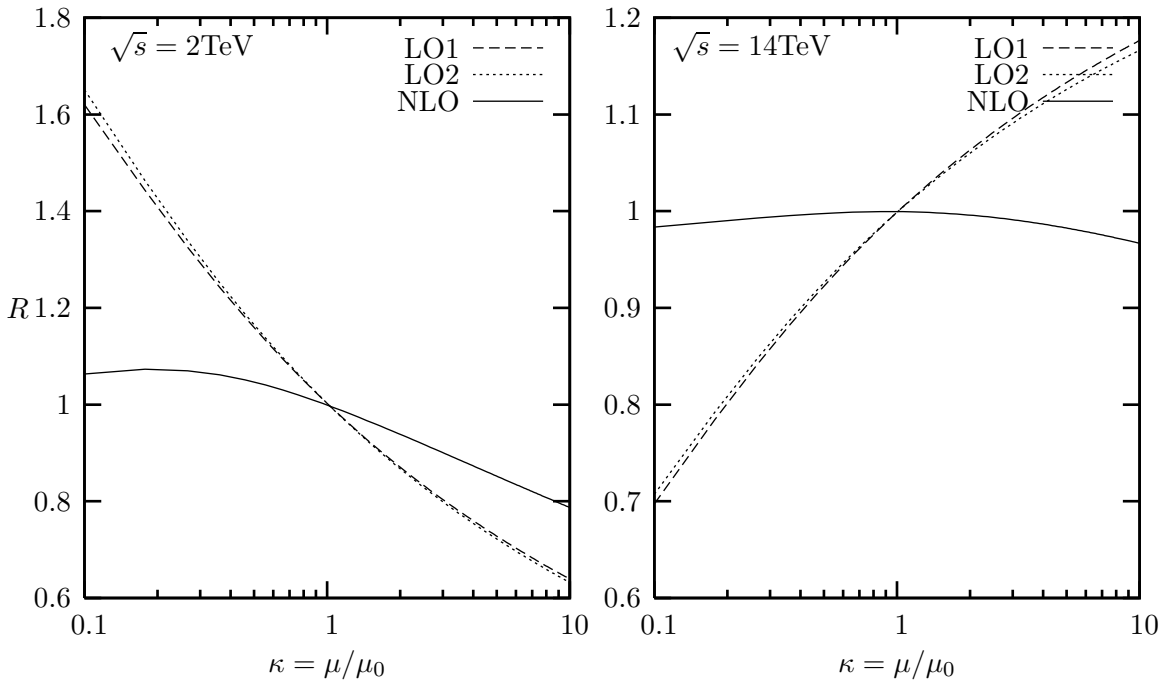

FIG. 6: The renormalization and factorization scale dependence of the leading order and next-to-leading order cross sections at Tevatron (left graph) and at LHC (right graph).

and the K factors in Fig. 8, respectively.

V. TRANSVERSE MOMENTUM DISTRIBUTION

In this section we investigate the transverse momentum distribution of the slepton. At Born level the slepton is kept at zero q_T due to momentum conservation and the distribution is proportional to $\delta^2(\boldsymbol{q}_T)$. Thus the leading order distribution at non-zero q_T belongs to $\mathcal{O}(\alpha_s)$, where momentum conservation is retained by the additional parton emitted. The distribution can be obtained by integrate out y from the differential cross section given in Section III. However, this fixed order result is only valid when q_T is not too small compared with the mass of the slepton m. If $q_T \ll m$, the corresponding parton emitted would be either soft or collinear to one of the initial partons. In consequence, large logarithms like $\ln(m^2/q_T^2)$ will appear and will dominate the cross section for sufficiently small q_T. In general, there should be double logarithms for each gluon attached to the initial quarks due to the overlap of soft region and collinear region. As a result, the perturbative expansion would be controlled by $\alpha_s \ln^2(m^2/q_T^2)$ rather than α_s. The convergence of the perturbation

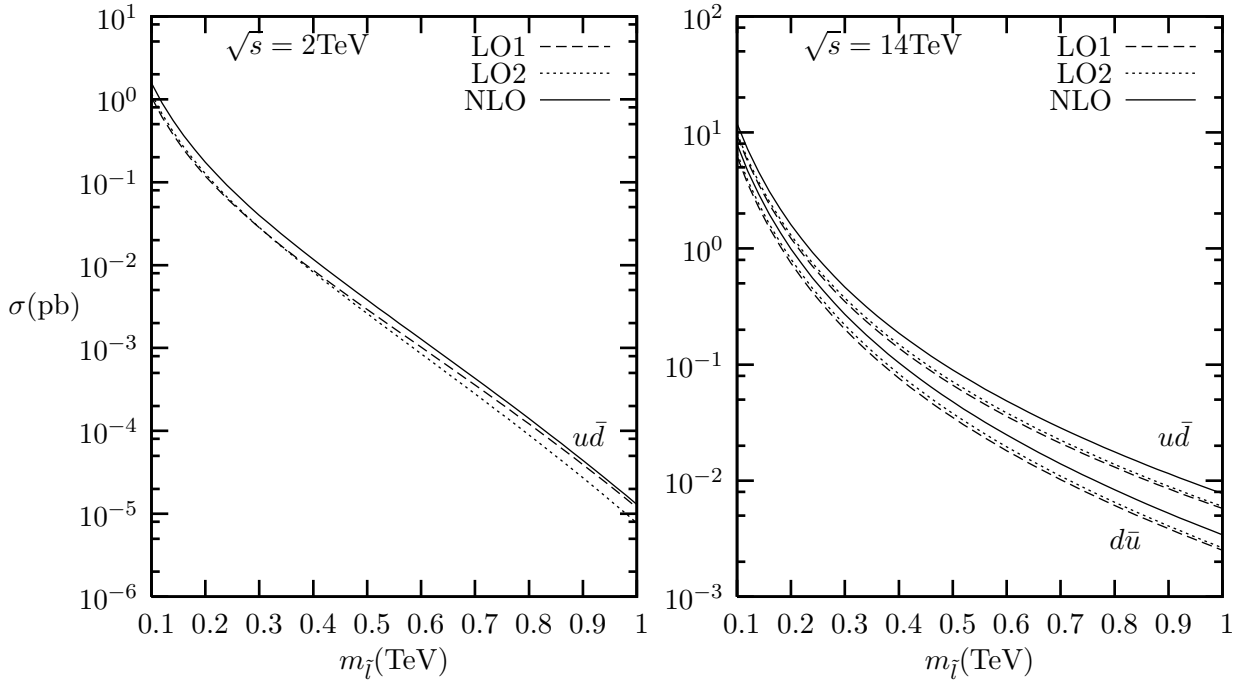

FIG. 7: The cross sections for charged slepton production at the Tevatron (left) and the LHC (right).

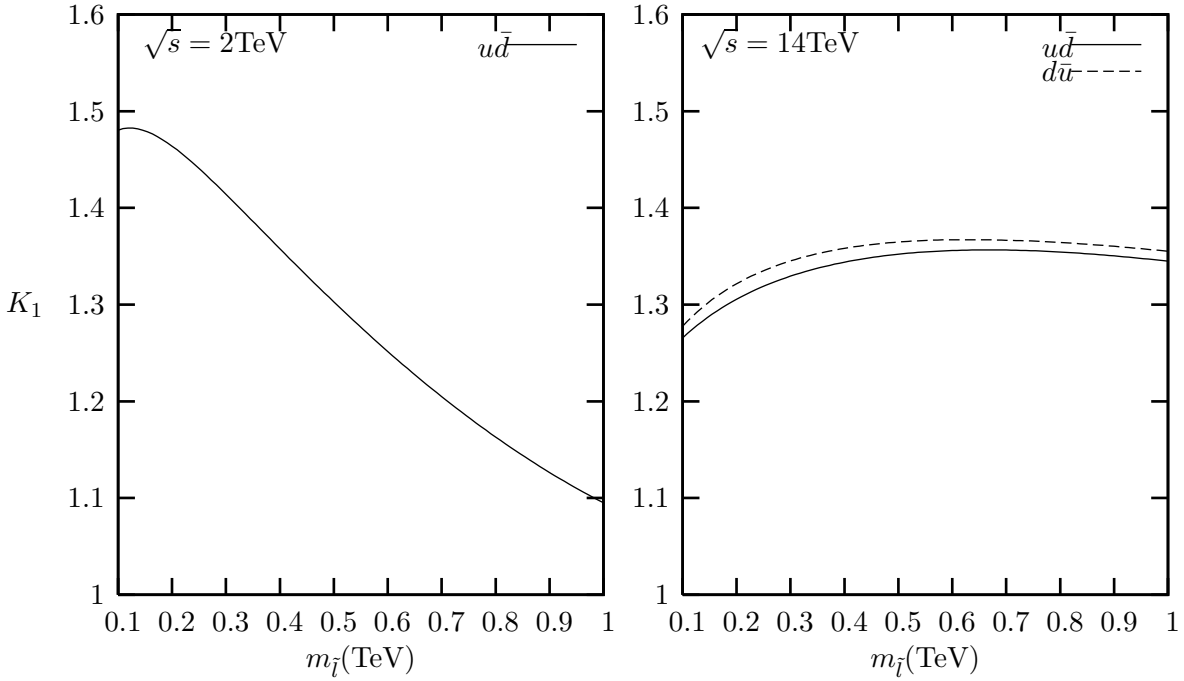

FIG. 8: The K factor (K_1) for charged slepton production at the Tevatron (left) and the LHC (right).

series will be spoiled if $\alpha_s \ln^2(m^2/q_T^2)$ approaches unity.

The problem arising at small q_T can also be seen from the fact that the fixed order cross section is singular as $q_T \to 0$. For later use, we define the asymptotic part of the differential cross section at small q_T to be the terms which are at least as singular as $1/q_T^2$ when $q_T \to 0$. At $\mathcal{O}(\alpha_s)$, the asymptotic expression can be isolated from the expressions obtained in section III:

$$\frac{\mathrm{d}\sigma}{\mathrm{d}q_T^2 \mathrm{d}y}(\mathrm{asym}) = \frac{1}{2}\sigma_0 \frac{\alpha_s}{\pi}\frac{1}{q_T^2}\Bigg\{ f_{\alpha/A}(x_1^0,\mu_f) f_{\beta/B}(x_2^0,\mu_f)\left(2C_F \ln\frac{m^2}{q_T^2} - 3C_F\right) + (P\circ f)_{\alpha/A}(x_1^0,\mu_f) f_{\beta/B}(x_2^0,\mu_f) + f_{\alpha/A}(x_1^0,\mu_f)(P\circ f)_{\beta/B}(x_2^0,\mu_f)\Bigg\}, \tag{36}$$

where $\sigma_0 = \dfrac{\pi}{12s}\lambda'^2$.

A. Resummation of large logarithms

In order to make use of the perturbation theory with the existence of large logarithms at each order, one must reorganize the perturbative expansion to resum the large terms. It was first shown by Dokshitzer, Diakonov and Troyan (DDT) [10] that in the double leading logarithm approximation (DLLA), terms like $\alpha_s^n \ln^{2n-1}(m^2/q_T^2)/q_T^2$ can be resummed into a Sudakov form factor. However, this result relies on the assumption that the emitted gluons are both soft and collinear and their transverse momenta are strongly ordered. With the over-constrained phase space, the resulting distribution is over-suppressed at small q_T. This implies that the subleading logarithms are also important and need to be resummed too. The subleading logarithms correspond to the phase space configurations in which some of the emitted gluons are not so soft or collinear. In this case, the transverse momentum conservation must be imposed, which is implemented in the b-space formalism introduced by Parisi and Petronzio [11]. Collins and Soper [12] improved the b-space formalism to resum all the terms like $\alpha_s^n L^r$ $(r = 0, ..., 2n-1)$ based on the renormalization group equation (RGE) method, where L represents the large logarithms. In this framework, Collins, Soper and Sterman (CSS) [13] derived a resummation formula for the transverse momentum distributions of the vector bosons produced in Drell-Yan processes. This formalism, often refered to as the CSS formalism, has also been applied to many other processes.

In the CSS formalism, the differential cross section we are considering can be written as

$$\frac{\mathrm{d}\sigma}{\mathrm{d}q_T^2\mathrm{d}y} = \frac{\mathrm{d}\sigma}{\mathrm{d}q_T^2\mathrm{d}y}(\text{resum}) + Y(q_T, m, x_1^0, x_2^0), \tag{37}$$

where the resummed part can be expressed as an inverse Fourier transformation

$$\begin{aligned}\frac{\mathrm{d}\sigma}{\mathrm{d}q_T^2\mathrm{d}y}(\text{resum}) &= \sum_{\alpha,\beta}\frac{1}{2}\sigma_0\frac{1}{2\pi}\int \mathrm{d}^2\boldsymbol{b}\exp\left(i\boldsymbol{b}\cdot\boldsymbol{q}_T\right)W_{\alpha\beta}(b, m, x_1^0, x_2^0) \\ &= \sum_{\alpha,\beta}\frac{1}{2}\sigma_0\int_0^\infty b\mathrm{d}bJ_0(bq_T)W_{\alpha\beta}(b, m, x_1^0, x_2^0),\end{aligned} \tag{38}$$

where $\boldsymbol{b}$ is the impact parameter conjugating to $\boldsymbol{q}_T$, J_0 is zero order Bessel function of the first kind, and

$$\begin{aligned}W_{\alpha\beta}(b, m, x_1^0, x_2^0) = \tilde{f}_{\alpha/A}(x_1^0, C_3/b)\tilde{f}_{\beta/B}(x_2^0, C_3/b) \\ \times\exp\left\{-\int_{C_1^2/b^2}^{C_2^2m^2}\frac{\mathrm{d}\bar{\mu}^2}{\bar{\mu}^2}\left[\ln\frac{C_2^2m^2}{\bar{\mu}^2}A(\alpha_s(\bar{\mu})) + B(\alpha_s(\bar{\mu}))\right]\right\}.\end{aligned} \tag{39}$$

Here $C_i (i = 1, 2, 3)$ are constants of order 1 which are by convention [13] chosen to be

$$C_1 = C_3 = 2e^{-\gamma_E} \equiv b_0,\ C_2 = 1, \tag{40}$$

and $\tilde{f}$ is the convolution of the PDFs and the coefficient functions C

$$\tilde{f}_{\alpha/h}(x, \mu) = \sum_\gamma\int_x^1\frac{\mathrm{d}z}{z}C_{\alpha\gamma}(z, \alpha_s(\mu))f_{\gamma/h}(x, \mu), \tag{41}$$

and the coefficients A, B and C can be expanded to series in α_s

$$A(\alpha_s) = \sum_{n=1}^\infty A^{(n)}\left(\frac{\alpha_s}{\pi}\right)^n, \tag{42}$$

$$B(\alpha_s) = \sum_{n=1}^\infty B^{(n)}\left(\frac{\alpha_s}{\pi}\right)^n, \tag{43}$$

$$C_{\alpha\beta}(z, \alpha_s) = \sum_{n=0}^\infty C_{\alpha\beta}^{(n)}(z)\left(\frac{\alpha_s}{\pi}\right)^n, \tag{44}$$

and they can be calculated order by order in perturbative theory. The lowest order coefficients can be extracted from the asymptotic expression above

$$A^{(1)} = C_F = \frac{4}{3}, \qquad B^{(1)} = -\frac{3}{2}C_F = -2, \tag{45}$$

$$C_{\alpha\beta}^{(0)}(z) = \delta_{\alpha\beta}\delta(1 - z). \tag{46}$$

With these coefficients, we can actually sum up all terms like $\alpha_s^n L^{2n-1}$ and $\alpha_s^n L^{2n-2}$.

The another term in Eq. (37), the Y term, is the remaining contributions which are not resummed. Since it contains no large logarithms, it can be reliably calculated in perturbation theory. In fact, according to the definition of the asymptotic part mentioned above, one can immediately see that

$$Y = \frac{\mathrm{d}\sigma}{\mathrm{d}q_T^2 \mathrm{d}y}(\text{pert}) - \frac{\mathrm{d}\sigma}{\mathrm{d}q_T^2 \mathrm{d}y}(\text{asym}). \tag{47}$$

However, the resummed part is still not able to be calculated perturbatively. The reason is that in Eq. (38), the integral over the impact parameter b extends to infinity, while the integrand involves the strong coupling constant α_s and the PDFs at scale b_0/b, where they are not well defined if b is large enough so that b_0/b enters non-perturbative region.

Many prescriptions have been developed regarding this problem, and we will show two approaches here. Collins, Soper and Sterman, in their original paper [13], suggested that one can use a cut-off $b_{\max}$ and regard the effects from $b > b_{\max}$ as non-perturbative input. Practically, they replacing $W(b)$ in Eq. (38) by

$$\widetilde{W}(b) = W(b_*) F_{\mathrm{NP}}(b), \tag{48}$$

where

$$b_* = \frac{b}{\sqrt{1 + (b/b_{\max})^2}}, \tag{49}$$

and $F_{\mathrm{NP}}(b)$ parameterizes the non-perturbative effects. Since b_* never exceeds $b_{\max}$, $W(b_*)$ can be calculated perturbatively, and the theoretical uncertainty mainly relies on the function F_{NP}. Recently, Landry, Brock, Nadolsky and Yuan (BLNY) [14] proposed the form

$$F_{\mathrm{NP}} = \exp\left\{-b^2\left[g_1 + g_2 \ln\frac{m}{2Q_0} + g_1 g_3 \ln(100 x_1^0 x_2^0)\right]\right\}. \tag{50}$$

They take $b_{\max} = 0.5\mathrm{GeV}^{-1}$, $Q_0 = 1.6\mathrm{GeV}$ and the parameters $g_i (i = 1, 2, 3)$ are fitted to the available Drell-Yan data, which are given by

$$g_1 = 0.21, \qquad g_2 = 0.68, \qquad g_3 = -0.60. \tag{51}$$

One of the largest disadvantages of the b_* prescription is that it alters the W function in the perturbative region $b < b_{\max}$. Regarding this, Qiu and Zhang (QZ) [15] proposed

another prescription so that $W(b)$ is kept unchanged for $b < b_{\rm max}$. Namely, they chose

$$\widetilde{W}(b) = \begin{cases} W(b) & b \le b_{\rm max}, \\ W(b_{\rm max}) F_{\rm NP}(b) & b > b_{\rm max}, \end{cases} \tag{52}$$

where $F_{\rm NP}$ takes the form

$$F_{\rm NP}(b) = \exp\left\{ -\ln\frac{m^2 b_{\rm max}^2}{b_0^2} \left[g_1 \left((b^2)^\alpha - (b_{\rm max}^2)^\alpha \right) + g_2 (b^2 - b_{\rm max}^2) \right] - \bar{g}_2 (b^2 - b_{\rm max}^2) \right\}. \tag{53}$$

The parameters g_1 and α are fixed by the continuity of the first and second derivative of $\widetilde{W}$ at $b = b_{\rm max}$, while g_2 and $\bar{g}_2$ are determined from experiments. In the numerical evaluation, we will use both above methods and compare their results.

B. Numerical results

In the numerical evaluation of the transverse momentum distribution, we take the renomalization and factorization scale for the fixed order expressions to be $\mu_r = \mu_f = \sqrt{m^2 + q_T^2}/2$. For simplicity, we only show the results for $d\bar{d}$ initial states as an example. The results for other initial states are similar. We use the CTEQ PDFs throughout this section.

According to the previous analysis, the differential cross section with respect to q_T^2 and y can be formally written as

$$\frac{{\rm d}\sigma}{{\rm d}q_T^2 {\rm d}y}({\rm total}) = \frac{{\rm d}\sigma}{{\rm d}q_T^2 {\rm d}y}({\rm resum}) + \frac{{\rm d}\sigma}{{\rm d}q_T^2 {\rm d}y}({\rm pert}) - \frac{{\rm d}\sigma}{{\rm d}q_T^2 {\rm d}y}({\rm asym}). \tag{54}$$

At small q_T, the asymptotic part and the perturbative part cancel each other, and the resummed part dominates the distribution. At large q_T, the difference between the resummed part and the asymptotic part belongs to higher orders in α_s, so the perturbative predictions are recovered. Since the perturbative part and the asymptotic part can be reliably calculated within perturbation theory, the only ambiguity comes from the resummed part due to the non-perturbative issue. So we shall compare the results of the different approaches to the non-perturbative parametrization for the reliable predictions.

With the two b-space prescriptions at hand (BLNY and QZ), we first compare the integrand of the Bessel transformation $b\widetilde{W}(b)$. We plot this function for a sneutrino with mass $m = 200$ GeV and rapidity $y = 0$ in Fig. 9. The solid curves represent the BLNY results, while the dashed and the dotted curves correspond to the the QZ prescription with two

choices of g_2: $g_2 = 0$ (no power corrections) and $g_2 \log(m^2 b_{\rm max}^2/b_0^2) = 0.8{\rm GeV}^2$ (fitted power corrections), respectively. The parameter $\bar{g}_2$ is always taken to be zero. From Fig. 9, we

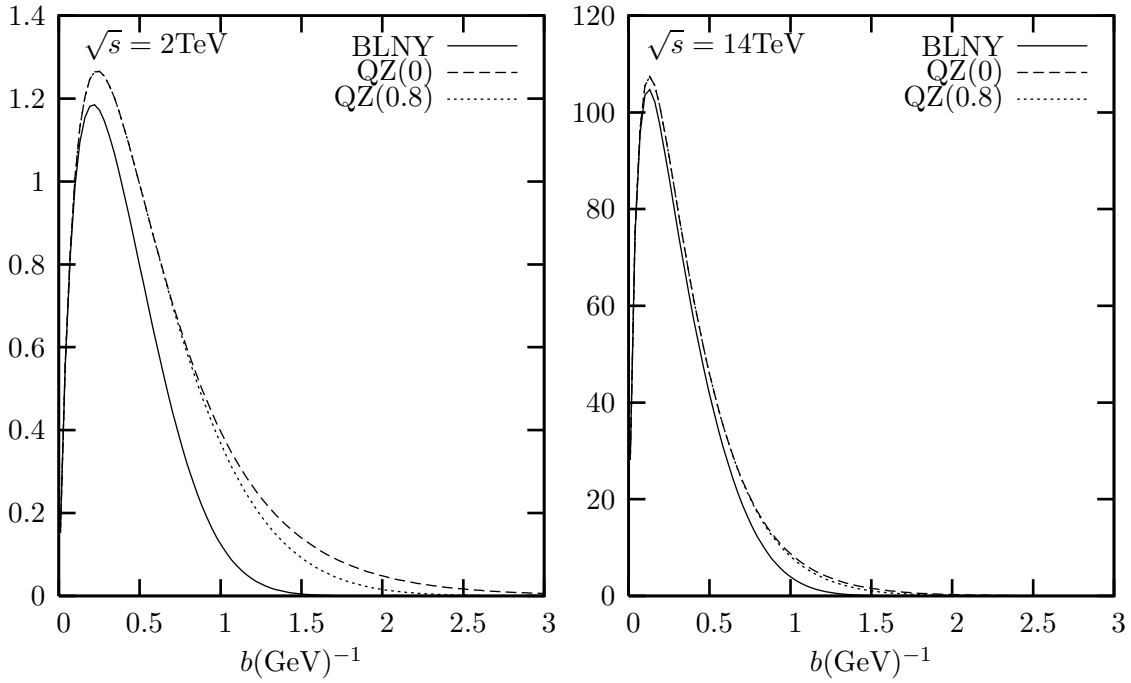

FIG. 9: Integrand of the b-integral (without the Bessel function) as a function of b for $m = 200$ GeV and $y = 0$ at the Tevatron (left) and the LHC (right).

can see that at the Tevatron, the BLNY parametrization notably changes the shape of the function for $b < b_{\rm max}$, and shows a sharper decrease than the one of QZ. As a result, the resummed differential cross sections for the two approaches will differ at small q_T (at larger q_T the impact of large b region gets smaller due to the Bessel function). On the other hand, the QZ parametrization itself is insensitive to the value of g_2. At the LHC, as shown in the right graph of Fig. 9, the difference is quite small, and the resummed cross sections are expected to agree to each other. Furthermore, the shape of the function is "narrower" at the LHC than the one at the Tevatron, i.e., the contributions from large b region to the integral at the LHC are smaller than the ones at the Tevatron. So we conclude that the predictions at the LHC is more reliable than the ones at the Tevatron. In Fig. 10, we plot the corresponding differential cross sections according to the two approaches. As discussed above, the results are slightly different at Tevatron and agree quite well at LHC. In the following calculations, we will adopt the QZ prescription and take $g_2 = 0$.

In Fig. 11, we plot the various parts of the differential cross section in Eq. (54) for rapidity

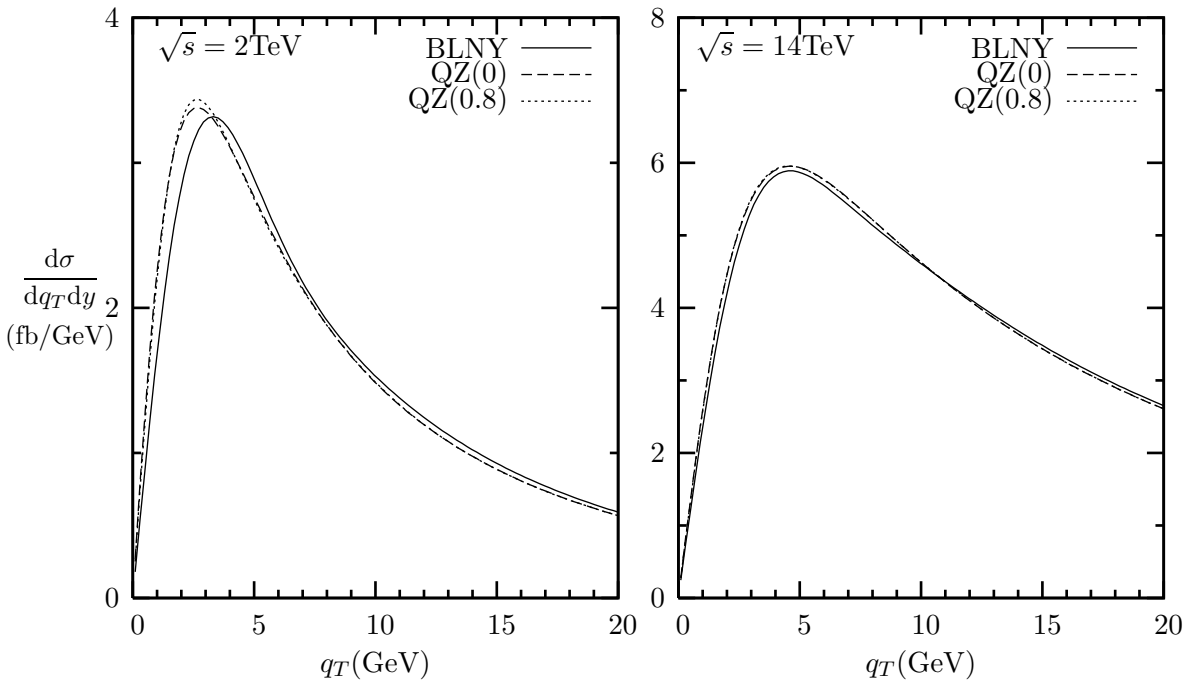

FIG. 10: Comparison of the resummed differential cross sections for $m = 200$ GeV and $y = 0$ at the Tevatron (left) and the LHC (right).

$y = 0$ at the Tevatron and the LHC. The mass of the sneutrino is taken to be 200 GeV. The solid, dashed, dotted and dot-dashed curves correspond to the total result, the resummed part, the perturbative part and the asymptotic part, respectively. Quantitatively, the perturbative and the asymptotic cross sections agree very well at small transverse momentum. On the other hand, the resummed and the asymptotic part are not cancelled completely at high q_T due to the higher order effects included in the resummed one, so that the total one and the perturbative one will differ at large q_T. This can be considered as the theoretical uncertainties. In principle, one can return to the perturbative result for $q_T > q_T^{\rm cut}$, where $q_T^{\rm cut}$ is arbitrarily chosen in the intermediate q_T region. However, in order to make the transition smooth, one must introduce some kinds of matching procedure which could also lead to uncertainties. In our work, we will use the resummed cross section from small q_T to large q_T.

Having settled down the technical issues, we now turn to show the predictions for the transverse momentum distributions of the slepton. For the y integral, the kinematic range

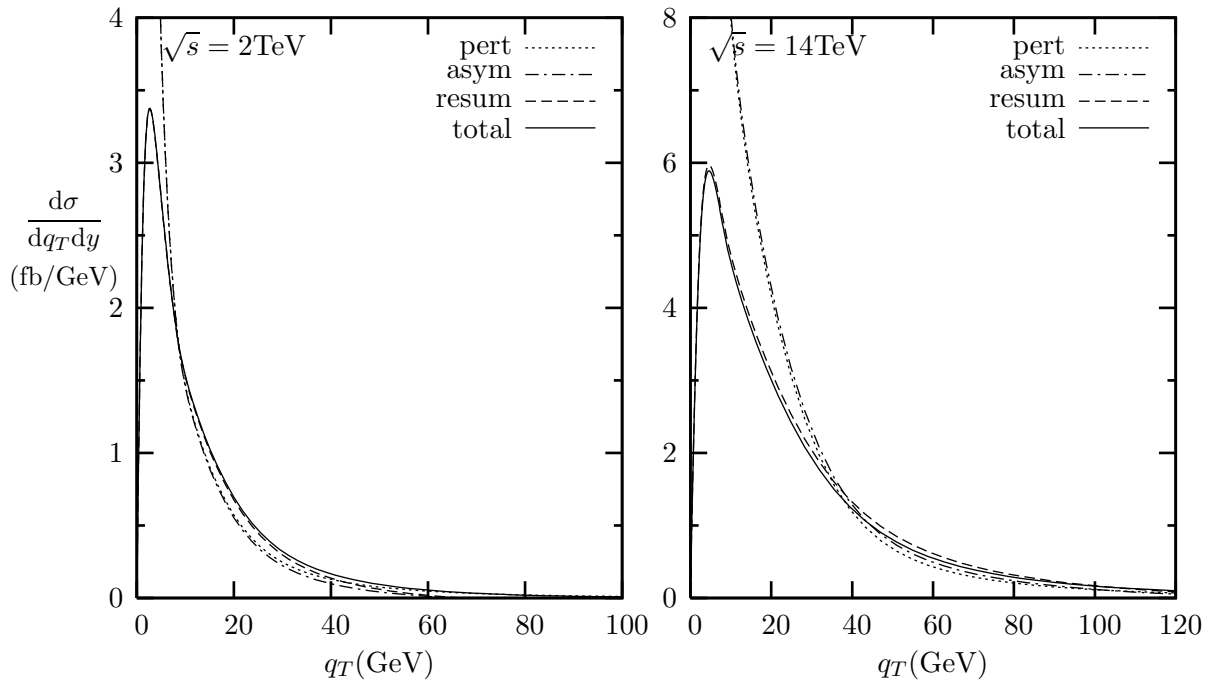

FIG. 11: The distribution with respect to the transverse momentum and the rapidity of the sneutrino from $d\bar{d}$ channel for central rapidity $y = 0$ at the Tevatron (left graph) and the LHC (right graph). The mass of the sneutrino is taken to be 200 GeV.

should be

$$|y| \leq \text{arccosh}\left(\frac{1+\tau}{2\sqrt{\tau + q_T^2/s}}\right). \tag{55}$$

In Fig. 12 we plot the transverse momentum distribution of the sneutrino from the $d\bar{d}$ channel at the Tevatron and the LHC separately. The mass of the sneutrino is taken to be 200 GeV, 400 GeV, 600 GeV, respectively. The peaks of the distribution appear at about 3 GeV at the Tevatron and about 5 GeV at the LHC. The differential cross sections decrease sharply with the increase of q_T, which indicates that most events will happen in the relatively low q_T region, where the resummation effects are essential. For example, about 80 percent of events lie in the $q_T < 20$ GeV region at the Tevatron, while at the LHC the range is $q_T < 40$ GeV. Therefore, the precise theoretical predictions for the distribution in the small q_T region are very important, which can help the selection of the the experimental cuts for better background rejection.

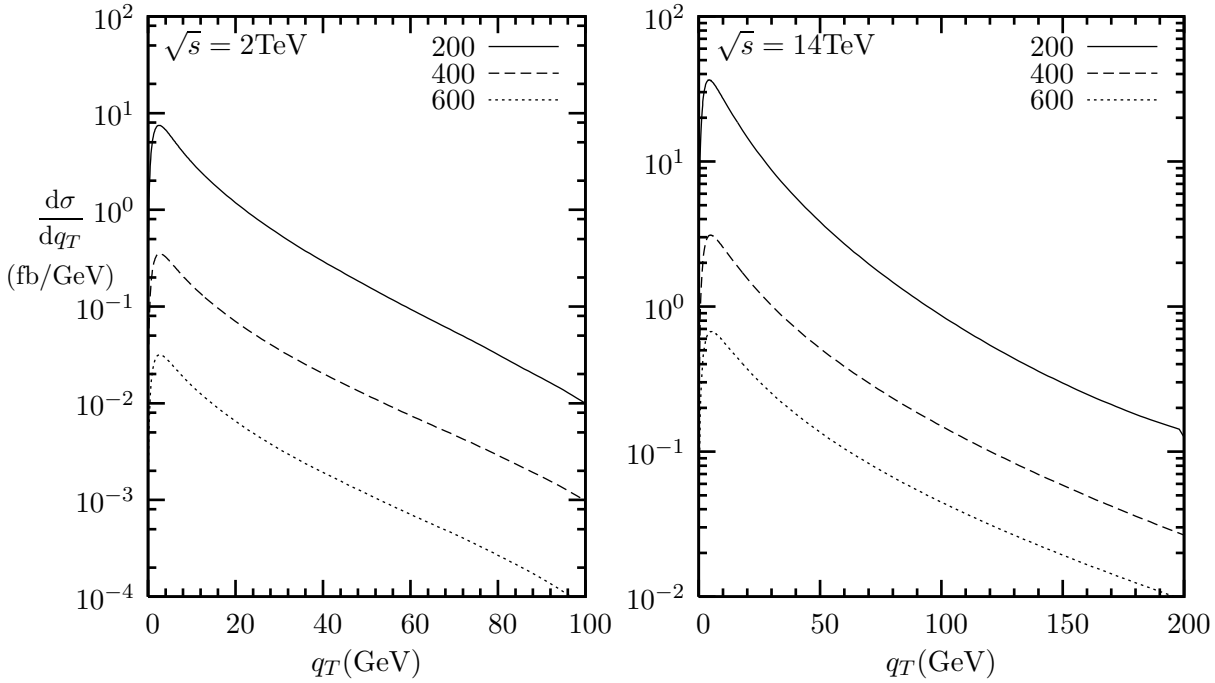

FIG. 12: The transverse momentum distribution of the sneutrino from $d\bar{d}$ channel at the Tevatron (left graph) and the LHC (right graph). The mass of the sneutrino is taken to be 200 GeV, 400 GeV, 600 GeV, as labeled in the figure.

VI. SUMMARY

In summary, we have calculated the next-to-leading order total cross section and transverse momentum distribution of a single slepton in the MSSM without R-parity, including all-order soft gluon resummation effects. For the total cross section, our results are consistent with the results of Ref. [9]. We update their numerical results with the updated version of the parton distribution functions and find that the discrepancy between the different sets of PDFs has been decreased compared with the previous version. Also, we find that the factorization and renormalization scale dependece in next-to-leading order is much smaller than the leading-order results. For the transverse momentum distribution, we resummed the large logarithms at small transverse momentum. Combined with the fixed order calculations, we give consistent predictions for both small q_T and large q_T. We also compared two approaches to the non-perturbative parametrization and found that the results are slightly different at the Tevatron and are in good agreement at the LHC. Our result can be useful to the simulation of the events and to the future collider experiments.

Acknowledgments

We would like to thank Jianwei Qiu for very helpful discussions. This work was supported in part by the National Natural Science Foundation of China, under grant Nos. 10421003 and 10575001, and the Key Grant Project of Chinese Ministry of Education, under grant NO. 305001.

---

[1] R. Barbier *et al.*, arXiv:hep-ph/0406039.

[2] M. Chemtob, Prog. Part. Nucl. Phys. **54**, 71 (2005) [arXiv:hep-ph/0406029].

[3] S. Dimopoulos and L. J. Hall, Phys. Lett. B **207**, 210 (1988).

V. D. Barger, G. F. Giudice and T. Han, Phys. Rev. D **40**, 2987 (1989).

G. F. Giudice *et al.*, arXiv:hep-ph/9602207.

E. Accomando *et al.* [ECFA/DESY LC Physics Working Group], Phys. Rept. **299**, 1 (1998) [arXiv:hep-ph/9705442].

J. Erler, J. L. Feng and N. Polonsky, Phys. Rev. Lett. **78**, 3063 (1997) [arXiv:hep-ph/9612397].

J. Kalinowski, R. Ruckl, H. Spiesberger and P. M. Zerwas, Phys. Lett. B **406**, 314 (1997) [arXiv:hep-ph/9703436].

[4] S. Dimopoulos, R. Esmailzadeh, L. J. Hall and G. D. Starkman, Phys. Rev. D **41**, 2099 (1990).

[5] H. K. Dreiner and G. G. Ross, Nucl. Phys. B **365**, 597 (1991).

B. Allanach *et al.* [R parity Working Group Collaboration], arXiv:hep-ph/9906224.

H. K. Dreiner, P. Richardson and M. H. Seymour, JHEP **0004**, 008 (2000) [arXiv:hep-ph/9912407].

A. Datta, J. M. Yang, B. L. Young and X. Zhang, Phys. Rev. D **56**, 3107 (1997) [arXiv:hep-ph/9704257].

J. M. Yang *et al.*, arXiv:hep-ph/9802305.

R. J. Oakes, K. Whisnant, J. M. Yang, B. L. Young and X. Zhang, Phys. Rev. D **57**, 534 (1998) [arXiv:hep-ph/9707477].

E. L. Berger, B. W. Harris and Z. Sullivan, Phys. Rev. Lett. **83**, 4472 (1999) [arXiv:hep-ph/9903549].

T. Plehn, Phys. Lett. B **488**, 359 (2000) [arXiv:hep-ph/0006182].

[6] J. Butterworth and H. K. Dreiner, Nucl. Phys. B **397**, 3 (1993) [arXiv:hep-ph/9211204].

[7] G. Moreau, M. Chemtob, F. Deliot, C. Royon and E. Perez, Phys. Lett. B **475**, 184 (2000) [arXiv:hep-ph/9910341].

F. Deliot, G. Moreau and C. Royon, Eur. Phys. J. C **19**, 155 (2001) [arXiv:hep-ph/0007288].

[8] H. K. Dreiner, P. Richardson and M. H. Seymour, Phys. Rev. D **63**, 055008 (2001) [arXiv:hep-ph/0007228].

[9] D. Choudhury, S. Majhi and V. Ravindran, Nucl. Phys. B **660**, 343 (2003) [arXiv:hep-ph/0207247].

[10] Y. L. Dokshitzer, D. Diakonov and S. I. Troian, Phys. Rept. **58**, 269 (1980).

[11] G. Parisi and R. Petronzio, Nucl. Phys. B **154**, 427 (1979).

[12] J. C. Collins and D. E. Soper, Nucl. Phys. B **193**, 381 (1981) [Erratum-ibid. B **213**, 545 (1983)].

J. C. Collins and D. E. Soper, Nucl. Phys. B **197**, 446 (1982).

[13] J. C. Collins, D. E. Soper and G. Sterman, Nucl. Phys. B **250**, 199 (1985).

[14] F. Landry, R. Brock, P. M. Nadolsky and C. P. Yuan, Phys. Rev. D **67**, 073016 (2003) [arXiv:hep-ph/0212159].

[15] J. w. Qiu and X. f. Zhang, Phys. Rev. D **63**, 114011 (2001) [arXiv:hep-ph/0012348].